

**Experimental and theoretical study of the double-core-hole hypersatellite Auger spectrum of Ne**

G. Goldsztejn,<sup>1,2,\*</sup> R. Püttner,<sup>3</sup> L. Journal,<sup>2,4</sup> R. Guillemin,<sup>2,4</sup> O. Travnikova,<sup>2,4</sup> B. Cunha de Miranda,<sup>2</sup> I. Ismail,<sup>2</sup> S. Carniato,<sup>2</sup> P. Selles,<sup>2</sup> D. Céolin,<sup>4</sup> A. F. Lago,<sup>5</sup> R. Feifel,<sup>6</sup> P. Lablanquie,<sup>2</sup> F. Penet,<sup>2</sup> M. N. Piancastelli,<sup>2,7</sup> M. Simon,<sup>2,4</sup> and T. Marchenko<sup>2,4</sup>

<sup>1</sup>Max-Born-Institut, Max-Born-Straße 2A, 12489 Berlin, Germany

<sup>2</sup>Sorbonne Universités, UPMC Univ Paris 06, CNRS, UMR 7614, Laboratoire de Chimie Physique-Matière et Rayonnement, F-75005 Paris, France

<sup>3</sup>Fachbereich Physik, Freie Universität Berlin, Arnimallee 14, D-14195 Berlin, Germany

<sup>4</sup>Synchrotron SOLEIL, l'Orme des Merisiers, Saint-Aubin, BP 48, F-91192 Gif-sur-Yvette Cedex, France

<sup>5</sup>Centro de Ciências Naturais e Humanas, Universidade Federal do ABC (UFABC), Rua Santa Adélia 166, 09210-170, Santo André, SP, Brazil

<sup>6</sup>Department of Physics, University of Gothenburg, SE-412 96 Gothenburg, Sweden

<sup>7</sup>Department of Physics and Astronomy, Uppsala University, P.O. Box 516, SE-751 20 Uppsala, Sweden

(Received 14 May 2017; published 19 July 2017)

We present the hypersatellite Auger spectrum of neon which contains the decay transitions of the  $K^{-2}$ ,  $K^{-2}V$ ,  $K^{-2}L^{-1}$ ,  $K^{-2}L^{-1}V$ , and  $K^{-1}L^{-1}V$  states. The Auger decays of these types of core-hole states show different line shapes and linewidths which can be distinguished due to the high experimental resolution available for the present experiments. The individual Auger transitions are assigned based on various approaches. Complementary calculations are performed to assign the  $K^{-2}L^{-1} \rightarrow K^{-1}L^{-3}$  and the  $K^{-2}L^{-1}V \rightarrow K^{-1}L^{-3}V$  Auger transitions. Based on the obtained results we were able to derive the ratio for the double to single ionization yield.

DOI: [10.1103/PhysRevA.96.012513](https://doi.org/10.1103/PhysRevA.96.012513)

**I. INTRODUCTION**

Interaction of atoms and molecules with hard x-ray radiation has important applications in the fields of structural biology and coherent diffraction imaging [1]. Ionization of atomic core shells with single high-energy photons or through multiphoton x-ray absorption may lead to formation of double core holes (DCH) either through a direct photoionization or via a cascade relaxation. We have recently shown that in molecules a dissociative character of such DCH states can enable ultrafast fragmentation on femtosecond time scale [2]. The Auger decay of DCH states is a complicated process involving multiple decay channels. A thorough spectroscopic analysis required for disentanglement of the possible decay channels and assignment of exotic states involved will contribute to our understanding of the fundamental processes occurring in atoms and molecules irradiated with hard x-ray light. In this work we undertake the challenge to provide a comprehensive analysis of hypersatellite Auger spectrum using neon atom as a model system.

Electronic states with a double hole in the  $K$  shell in atoms were initially observed in nuclear reactions in the mid-20th century [3]. In particular cases, the nuclei of radioactive atoms may be able to capture a  $1s$  electron while the other  $1s$  electron is ejected into the continuum. The subsequent studies focused on the DCH electronic states, formed *via* different experimental processes: electron [4] or ion [5–7] collisions on several targets, bare ions interacting with metallic surfaces from which they attract electrons to create hollow ions [8–11], photoexcitation and photoionization using x-ray tubes [12], or synchrotron radiation [13,14].

Within the past decade, the study of DCH states acknowledged a substantial revival of interest mostly due to

the advent of x-ray free-electron lasers (X-FELs) on one side and synchrotron radiation sources coupled to advanced coincidence techniques on the other side. In the first case, the very short pulses (in the order of few fs) and the high number of photons per pulse, allowed multiphoton sequential absorption processes on time scales comparable to Auger decay. The electrons corresponding to DCH states were measured with time-of-flight detectors [15–17]. In the second case, the synchrotron radiation is used to create DCH states and the emitted electrons are measured in coincidence using a magnetic bottle [18–26]. When two holes are created as an intermediate state, they can be filled by a concerted or a sequential Auger decay. Although the former is less probable, we have recently shown that two electrons may fill the holes created simultaneously, while one electron is emitted into the continuum carrying the excess energy [27].

We have recently shown that it is also possible to study DCH states in direct photoionization using synchrotron radiation at high photon energy ( $h\nu = 2$  to 12 keV) and high photon flux [28]. Furthermore, in combination with high-resolution spectroscopy, this method provides also a detailed information on the lifetime of such states [28]. In our recent Letter [29], in addition to  $K^{-2}V$  DCH states ( $V =$  valence electron) observed in neon photoelectron spectra, we have presented the hypersatellite spectrum of the first Auger decay subsequent to the creation of DCH.

Previously, hypersatellites were extensively studied in x-ray fluorescence [30–32] and Auger electron spectra [33–36]. However, previous studies on neon [36] were not able to disentangle the multiple overlapping contributions due to the lack of experimental resolution. Calculations including only  $2S^e$  ionic final states did not provide a satisfactory agreement with the experiment. The discrepancy is related to the complexity of the Auger spectrum, which besides the decay of the  $K^{-2}V$  shake-up satellites and the  $K^{-2}$  shake-off satellites of the  $1s^{-1}$  ionization, contains also the Auger

\*gildas.goldsztejn@mbi-berlin.de

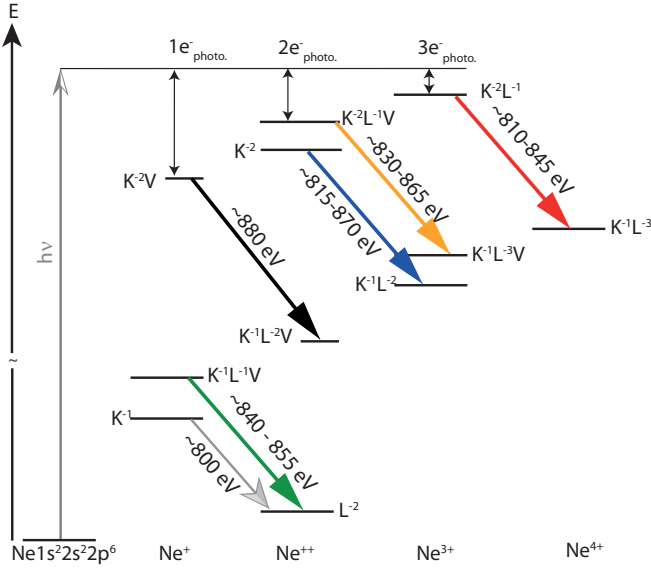


FIG. 1. Systematic sketch of the Auger processes subsequent to  $K^{-1}$ ,  $K^{-1}L^{-1}V$ ,  $K^{-2}$ ,  $K^{-2}V$ ,  $K^{-2}L^{-1}$ , and  $K^{-2}L^{-1}V$  ionization. The  $K^{-1}L^{-1}V \rightarrow L^{-2}$  Auger decays are indicated in green, the  $K^{-2} \rightarrow K^{-1}L^{-2}$  Auger decays in blue, the  $K^{-2}V \rightarrow K^{-1}L^{-2}V$  decays in black, the  $K^{-2}L^{-1}V \rightarrow K^{-1}L^{-3}V$  in orange, and the  $K^{-2}L^{-1} \rightarrow K^{-1}L^{-3}$  Auger decays in red. For the individual types of Auger decays the ranges of Auger energies are also given.

decay of the  $K^{-2}L^{-1}$  and  $K^{-2}L^{-1}V$  shake states as well as the participator decay of the  $K^{-1}L^{-1}V$  shake-up states. A schematic picture including the possible Auger decays of all these intermediate states, with their kinetic energy ranges, is presented in Fig. 1. We have already showed previously that decay of the different types of intermediate states can be distinguished by their linewidths and line shapes [29]; however, this was not sufficient to disentangle and assign all the different contributions. In the present work, we present a detailed assignment of neon hypersatellite spectrum based on different experimental and theoretical methods.

## II. EXPERIMENTAL DETAILS

The measurements of the hypersatellite Auger spectrum were performed at the GALAXIES beamline of the French national synchrotron radiation facility SOLEIL [37]. The utilized hard x-ray photoelectron spectroscopy (HAXPES) end station is thoroughly described in Ref. [38]. In short, the lens system of the analyzer is set parallel to the polarization vector of the linearly polarized photon beam. The presented Auger spectrum was measured using a photon energy of 2.3 keV because at this photon energy the photon flux of the beamline is at its maximum. The obtained overall experimental resolution amounts to  $250 \pm 10$  meV. It consists of an electronic Doppler broadening at room temperature  $\delta = 0.723(ET/M)^{1/2}$  meV [39] of  $\approx 80$  meV for 870 eV electrons (where  $E$  is the kinetic energy in eV,  $T$  is the temperature in K, and  $M$  is the mass of the atom in atomic mass unit) as well as a broadening due to the recoil of the ion of  $\approx 35$  meV [40]. However, the main contribution originates from the spectrometer resolution of  $235 \text{ meV} \pm 10 \text{ meV}$  that was

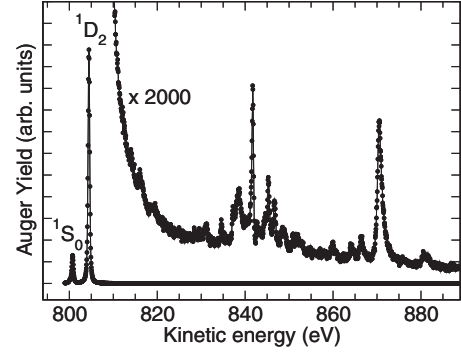


FIG. 2. Energy region of the  $1s^{-1} \rightarrow 2p^{-2}$  Auger decays of neon together with that of the hypersatellites. To visualize the hypersatellites in the corresponding energy region the intensity is multiplied by a factor of 2000.

deduced by fitting the  $KLL$  Auger spectrum of neon; see Fig. 2. In this fit procedure the lines were described with a Voigt function corresponding to a Lorentzian of 242 meV FWHM [29,41] convoluted with a Gaussian function representing the determined total experimental resolution. The kinetic-energy axis was calibrated using the  $1s^{-1} \rightarrow 2p^{-2}(^1D_2)$  normal Auger transition of neon at  $E_{\text{kin}} = 804.46$  eV [42].

## III. METHODS AND RESULTS

Figure 2 shows an overview spectrum of the hypersatellite Auger decays of neon together with the diagram lines of the  $Ne 1s^{-1} \rightarrow 2p^{-2}$  Auger decay which are used for calibration purposes. To visualize the hypersatellite Auger decays in this figure, the Auger intensity has been multiplied by a factor of 2000 in the corresponding energy range. The curve obtained in this way shows a continuously decreasing background which is due to the high-energy tail of the Lorentzian line shape of the  $1s^{-1} \rightarrow 2p^{-2}(^1D_2)$  normal Auger transition at  $E_{\text{kin}} = 804.46$  eV. This shows impressively the slow convergence of Lorentzian line shape to the zero level.

The detailed hypersatellite Auger spectrum after background subtraction is presented in Fig. 3. As discussed above in the context of Fig. 1, the Auger decays of the  $K^{-2}$ ,  $K^{-2}V$ ,  $K^{-2}L^{-1}$ ,  $K^{-2}L^{-1}V$ , and  $K^{-1}L^{-1}V$  states overlap in this energy region. The Auger decays of these states are distinguished in a fit analysis using the fact that the different types of Auger processes exhibit different line shapes and linewidths. These differences will be discussed in detail further below. In the fit analysis, the background is described by a linear part and a Lorentzian function representing the  $1s^{-1} \rightarrow 2p^{-2}(^1D_2)$  normal Auger transition. This background is removed in Fig. 3. Its dominating influence on the low-energy part of the spectrum limits the region accessible to the fit analysis and can be seen by the strong scattering of the data points. The Auger decays of the different intermediate states are described by colored subspectra. In detail, the  $K^{-1}L^{-1}V \rightarrow L^{-2}$  Auger decays are indicated in green filled with diagonal lines going from bottom left to top right, the  $K^{-2} \rightarrow K^{-1}L^{-2}$  Auger decays in blue filled with horizontal lines, the  $K^{-2}V \rightarrow K^{-1}L^{-2}V$  decays in black, the  $K^{-2}L^{-1}V \rightarrow K^{-1}L^{-3}V$  decays in orange filled with diagonal lines going from top left to bottom right, and the

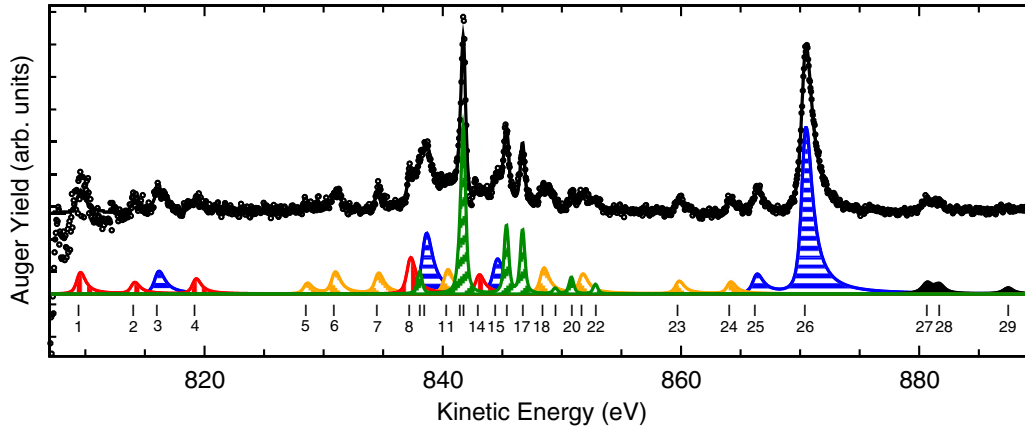


FIG. 3. Hypersatellite Auger spectrum of neon after subtracting the background obtained in the fit analysis. The solid line through the data points represents the fit result. The  $K^{-1}L^{-1}V \rightarrow L^{-2}$  Auger decays are indicated in green filled with diagonal lines going from bottom left to top right, the  $K^{-2} \rightarrow K^{-1}L^{-2}$  Auger decays in blue filled with horizontal lines, the  $K^{-2}V \rightarrow K^{-1}L^{-2}V$  decays in black, the  $K^{-2}L^{-1}V \rightarrow K^{-1}L^{-3}V$  decays in orange filled with diagonal lines going from top left to bottom right, and the  $K^{-2}L^{-1} \rightarrow K^{-1}L^{-3}$  Auger decays in red filled with vertical lines.

$K^{-2}L^{-1} \rightarrow K^{-1}L^{-3}$  Auger decays in red filled with vertical lines. Table I summarizes the kinetic energies obtained from the fits together with the assignments as well as theoretical values used to support the assignments. For a more convenient discussion, in Table I and in Fig. 3 the different transitions are labeled with numbers.

In the following we shall describe in more detail the arguments and methods used to distinguish and assign the different types of Auger decays.

#### A. Hypersatellites of $K^{-2}$ electronic states

The peaks corresponding to the hypersatellite Auger decays of  $K^{-2}$  electronic states can be identified based on three different arguments. First, they present a pronounced asymmetric PCI (postcollision interaction) line shape, as described thoroughly in Ref. [29]. In short, this strong asymmetry is caused by the typical energy sharing of the two electrons in case of double ionization with one photon. This sharing reflects a characteristic “U-shape” of the kinetic-energy distribution [19], i.e., the most probable way of energy sharing results in one fast and one slow electron. Such a slow photoelectron screens, during the subsequent Auger decay, the doubly charged ion core and accelerates the fast Auger electron, which causes a characteristic asymmetric line shape.

Second, as also discussed in Ref. [29], the lifetimes of the various types of core-ionized states are different due to the number of core holes as well as the number of valence electrons that can fill the created core holes. In the fit analysis the same parameter for the lifetime broadening was used for all  $K^{-2}$  DCH states resulting in the value  $\Gamma = 910 \pm 12$  meV. This broadening is due to the lifetimes of the  $K^{-2}$  intermediate state and of the  $K^{-1}L^{-2}$  final state. The obtained value for  $\Gamma$  is in perfect agreement with the theoretical results from Ref. [43] of 903 meV for the  $1s^{-2} \rightarrow 1s^{-1}2p^{-2}$  transitions and 907 meV for the  $1s^{-2} \rightarrow 1s^{-1}2s^{-1}2p^{-1}$  transitions. In contrast, the calculated value for the  $1s^{-2} \rightarrow 1s^{-1}2s^{-2}$  transition (peak 3) is 936 meV, slightly larger than the fit

value; it has, however, only a weak influence on the obtained fit value due to its low intensity.

A third argument for the assignment of hypersatellite Auger decay of  $K^{-2}$  states relies on the results of three different calculations [34,44,45], which provide a good agreement with each other in terms of Auger energies and branching ratios. For the transitions that are strong enough to be observed in Fig. 3 the theoretical results are summarized in Table II, together with the experimental results.

Based on above presented arguments we identify peaks 3, 9, 15, 25, and 26 as  $1s^{-2} \rightarrow 1s^{-1}2l^{-2}$  hypersatellite Auger decays indicated in blue filled with horizontal lines in Fig. 3. In the previous study of Southworth *et al.* [36] peaks 25 and 26 were presented as one broad spectral feature, peaks 9 and 15 were unresolved, and peak 3 was not observed. In Table II the experimental energy positions of these peaks match reasonably well the theoretical results. In particular, the agreement is very good in terms of energy positions and relative splittings with the most recent calculations of Liu *et al.* [44]. The experimental branching ratios agree also well with the theoretical results, with the exception of the  $1s^{-2} \rightarrow 1s^{-1}2s^{-1}2p^{-3}P^0(^2S)$  transition (peak 15) that is larger in experiment than in all theoretical approaches. However, this transition is in a spectral region where different states overlap so that we cannot give a definite explanation for this discrepancy. It is possible that the intensity of this transition is underestimated by theory. But it is also possible that it overlaps with one or more unresolved  $K^{-2}L^{-1} \rightarrow K^{-1}L^{-3}$  or  $K^{-2}L^{-1}V \rightarrow K^{-1}L^{-3}V$  Auger transition. So, for example, the theoretical kinetic energy of the  $1s^{-2}2p^{-1}(^2P) \rightarrow 1s^{-1}2p^{-3}(^1D)$  Auger transition is 845.970 eV, which is close to the experimental value; see Sec. III C. Beside this small uncertainty the good agreement with theory fully confirms the given assignment.

The discussed final states are formed by the states  $2p^{-2}(^1D)$ ,  $2p^{-2}(^1S)$ ,  $2s^{-1}2p^{-1}(^3P)$ ,  $2s^{-1}2p^{-1}(^1P)$ , and  $2s^{-2}(^1S)$  coupled to a  $1s^{-1}$  core hole. We would like to point out that the splittings between the state  $2p^{-2}(^1D)$  and  $2p^{-2}(^1S)$ ,  $2s^{-1}2p^{-1}(^3P)$ ,  $2s^{-1}2p^{-1}(^1P)$ , as well as  $2s^{-2}(^1S)$  for  $\text{Ne}^{2+}$  are 3.71 eV,

TABLE I. Summary of the observed transitions including their assignment. Given are the experimental and theoretical kinetic energies. The assignments of the transitions marked with “?” are tentative. The errors of the experimental line positions are estimated to be in the order of 100 meV. For more readability, the peak numbers are also indicated in Fig. 3.

Peak number	Kinetic energy (eV)	Hole type	Assignment	Theory (eV)
1	809.4	$K^{-2}L^{-1}$	$1s^{-2}2p^{-1}(^2P) \rightarrow 1s^{-1}2s^{-1}2p^{-2}(^1S)$	810.905 <sup>a</sup>
2	814.0	$K^{-2}L^{-1}$	$1s^{-2}2s^{-1}(^2S) \rightarrow 1s^{-1}2s^{-2}2p^{-1}(^1P)?$	?
3	816.0	$K^{-2}$	$1s^{-2}(^1S) \rightarrow 1s^{-1}2s^{-2}(^2S)$	816.95 <sup>b,c</sup>
4	819.1	$K^{-2}L^{-1}$	$1s^{-2}2p^{-1}(^2P) \rightarrow 1s^{-1}2s^{-1}2p^{-2}(^1D)$	817.134 <sup>a</sup>
5	828.5	$K^{-2}L^{-1}V$	$1s^{-2}2s^{-1}3p \rightarrow 1s^{-1}2s^{-2}2p^{-1}3p?$	?
6	830.8	$K^{-2}L^{-1}V$	$1s^{-2}2s^{-1}3p \rightarrow 1s^{-1}2s^{-2}2p^{-1}3p?$	?
7	834.5	$K^{-2}L^{-1}V$	$1s^{-2}2s^{-1}3p \rightarrow 1s^{-1}2s^{-2}2p^{-1}3p?$	?
8	837.2	$K^{-2}L^{-1}$	$1s^{-2}2s^{-1}(^2S) \rightarrow 1s^{-1}2s^{-1}2p^{-2}(^1S)$	837.844 <sup>a</sup>
9	838.4	$K^{-2}$	$1s^{-2} \rightarrow 1s^{-1}2s^{-1}2p^{-1}P^0(^2P^0)$	838.95 <sup>b,c</sup>
10	840.3	$K^{-2}L^{-1}V$	$1s^{-2}2s^{-1}3s(^1S) \rightarrow 1s^{-1}2s^{-2}2p^{-1}(^1P)3s?$	?
11	838.1	$K^{-1}L^{-1}V$	$1s^{-1}2p^{-1}3p^1(L) \rightarrow 2p^{-2}(^1S)$	837.93 <sup>d</sup>
12	841.4	$K^{-1}L^{-1}V$	$1s^{-1}2p^{-1}3p^1(H) \rightarrow 2p^{-2}(^1S)$	841.34 <sup>d</sup>
13	841.7	$K^{-1}L^{-1}V$	$1s^{-1}2p^{-1}3p^1(L) \rightarrow 2p^{-2}(^1D)$	841.64 <sup>d</sup>
14	842.9	$K^{-2}L^{-1}$	$1s^{-2}2s^{-1}(^2S) \rightarrow 1s^{-1}2s^{-1}2p^{-2}(^1D)$	844.073 <sup>a</sup>
15	844.4	$K^{-2}$	$1s^{-2} \rightarrow 1s^{-1}2s^{-1}2p^{-1}P^0(^2P^0)$	845.24 <sup>b,c</sup>
16	845.3	$K^{-1}L^{-1}V$	$1s^{-1}2p^{-1}3p^1(H) \rightarrow 2p^{-2}(^1D)$	845.05 <sup>d</sup>
17	846.7	$K^{-1}L^{-1}V$	$1s^{-1}2p^{-1}4p^1(L) \rightarrow 2p^{-2}(^1D)$	846.64 <sup>d</sup>
18	848.3	$K^{-2}L^{-1}V$	$1s^{-2}2s^{-1}3p(^3D) \rightarrow 1s^{-1}2p^{-2}3p(^4D)$	851.769 <sup>a</sup>
		$K^{-1}L^{-1}V$	$1s^{-1}2p^{-1}5p^1(L) \rightarrow 2p^{-2}(^1D)$	848.40 <sup>a</sup>
19	849.4	$K^{-1}L^{-1}V$	$1s^{-1}2p^{-1}6p^1(L) \rightarrow 2p^{-2}(^1D)$	849.37 <sup>a</sup>
20	850.8	$K^{-1}L^{-1}V$	$1s^{-1}2p^{-1}4p^1(H) \rightarrow 2p^{-2}(^1D)$	850.73 <sup>a</sup>
21	851.6	$K^{-2}L^{-1}V$	$1s^{-2}2p^{-1}3s(^3P) \rightarrow 1s^{-1}2s^{-1}2p^{-2}3s(^4P)$	852.310 <sup>a</sup>
22	852.8	$K^{-1}L^{-1}V$	$1s^{-1}2p^{-1}5p^1(H) \rightarrow 2p^{-2}(^1D)$	852.75 <sup>a</sup>
		$K^{-1}L^{-1}V$	$1s^{-1}2p^{-1}6p^1(H) \rightarrow 2p^{-2}(^1D)$	853.79 <sup>d</sup>
23	859.7	$K^{-2}L^{-1}V$	$1s^{-2}2p^{-1}3p(^3S) \rightarrow 1s^{-1}2p^{-3}3p(^2S)$	857.771 <sup>a</sup>
24	864.0	$K^{-2}L^{-1}V$	$1s^{-2}2p^{-1}3p(^3S) \rightarrow 1s^{-1}2p^{-3}3p(^2P)$	864.185 <sup>a</sup>
25	866.2	$K^{-2}$	$1s^{-2} \rightarrow 1s^{-1}2p^{-2}(^2S)$	866.42 <sup>b,c</sup>
26	870.4	$K^{-2}$	$1s^{-2} \rightarrow 1s^{-1}2p^{-2}(^2D)$	870.54 <sup>b,c</sup>
27	880.6	$K^{-2}V$	$1s^{-2}3p^1 \rightarrow 1s^{-1}2p^{-2}(^2D)3p^1$	880.936 <sup>a</sup>
28	881.7	$K^{-2}V$	$1s^{-2}3s^1 \rightarrow 1s^{-1}2p^{-2}(^2D)3s^1$	882.811 <sup>a</sup>
29	887.4	$K^{-2}V$	$1s^{-2}4p^1 \rightarrow 1s^{-1}2p^{-2}(^2D)3p^1$	886.636 <sup>a</sup>

<sup>a</sup>Present work.

<sup>b</sup>Reference [44].

<sup>c</sup>For additional theoretical results, see Table II.

<sup>d</sup>Calculated with Eq. (2) and the values given in Ref. [53].

22.2 eV, 32.69 eV, and 56.17 eV [46], respectively. These values are close to the splitting of the states with an additional Ne  $1s^{-1}$  core hole and show that the latter has only limited influence.

### B. Hypersatellites of $K^{-2}V$ electronic states

The only Auger decays of the  $K^{-2}V$  states allowed in the energy range of Fig. 3 are spectator and “shake” decays, while the participator decays are expected at much higher energies

TABLE II. Calculated kinetic energies,  $E_k$ , the relative kinetic energies compared to the final state  $1s^12s^22p^4(^2D)$ ,  $\Delta E$ , and the branching ratios given in percent, BR, for the five most intense and experimentally observed  $K^{-2} \rightarrow K^{-1}L^{-2}$  Auger transitions as obtained from different calculations. For comparison, the results of the present fit analysis are also given. The error bars for the experimental BR given in brackets are based on the statistical errors of the fit analysis. Systematic errors like an overlap with an unrecognized transition are not taken into account.

Final state	Peak number	Ref. [45]			Ref. [34]			Ref. [44]			Present experiment		
		$E_k$ (eV)	$\Delta E$ (eV)	BR	$E_k$ (eV)	$\Delta E$ (eV)	BR	$E_k$ (eV)	$\Delta E$ (eV)	BR	$E_k$ (eV)	$\Delta E$ (eV)	BR
$1s^12s^22p^4(^2D)$	26	872.4	0	61.26	872.2	0	49.2	870.54	0	66.16	870.4	0	54.9(1.6)
$1s^12s^22p^4(^2S)$	25	868.8	3.6	6.89	868.7	3.5	9.2	866.42	4.12	9.96	866.2	4.2	6.4(0.9)
$1s^12s^12p^5\ ^3P^0(^2S)$	15	844.1	28.3	0.41	844.3	27.9	1.1	845.22	25.32	2.19	844.4	26.0	11.2(1.2)
$1s^12s^12p^5\ ^1P^0(^2S)$	9	837.0	35.4	26.14	837.1	35.1	33.0	838.95	31.59	18.11	838.4	32.0	20.0(2.3)
$1s^12s^02p^6(^2S)$	3	812.6	59.8	5.84	812.9	59.3	7.0	816.95	53.59	3.19	816.0	54.4	7.5(1.5)

( $\sim 900$ – $930$  eV). The initial states of these Auger decays are singly ionized with a fast photoelectron emitted. As discussed in Ref. [29] this fast photoelectron leads to a negligible PCI effect and—as a consequence—to a symmetric Lorentzian line shape.

To determine the kinetic energies of the spectator and shake hypersatellites, we used the equivalent-core approximation. In this model, the kinetic energy of the Auger decay  $1s^{-2}nl \rightarrow 1s^{-1}2(s,p)^{-2}(2L)n'l'$  is given by

$$E_k(nl,2(s,p)^{-2}(2L)n'l') = E_k(2(s,p)^{-2}(2L)) + T_V - T_{V'}, \quad (1)$$

where  $E_k(2(s,p)^{-2}(2L))$  is the kinetic energy of the  $1s^{-2} \rightarrow 1s^{-1}2(s,p)^{-2}(2L)$  hypersatellite Auger decay. The term values  $T_V$  and  $T_{V'}$  are estimated using the  $Z+2$  and the  $Z+1$  approximation, respectively. In more detail,  $T_V$  is the term value of an electron in the  $nl$  orbital of the  $Z+2$  atom  $Mg^+$  in the configuration  $1s^22s^22p^6nl$  and  $T_{V'}$  is the term value of an electron in the  $n'l'$  orbital of the  $Z+1$  atom  $Na^{2+}$  in the configuration  $1s^22s^22p^4n'l'$ . In the case of  $nl = n'l'$  a spectator Auger decay occurs and in the case of  $nl \neq n'l'$  a shake process occurs. The term values of the respective states in  $Mg^+$  and  $Na^{2+}$  are tabulated in the NIST atomic spectra database [46].

In the fit analysis we have found that the peaks 27, 28, and 29 have a symmetric line shape; in Fig. 3 they are indicated in black. Based on this observation they are identified as Auger transitions of the type  $1s^{-2}nl \rightarrow 1s^{-1}2l^{-2}n'l'$ . To specify the transitions we employed Eq. (1) and obtained a kinetic energy of 881.04 eV for the  $1s^{-2}3s^1 \rightarrow 1s^{-1}2l^{-2}3s$  Auger transition and 880.29 eV for the  $1s^{-2}3p^1 \rightarrow 1s^{-1}2p^{-2}(2D)3p^1$  Auger transition. Based on these results peak 28 at a kinetic energy of 881.7 eV is assigned to the  $1s^{-2}3s^1 \rightarrow 1s^{-1}2p^{-2}(2D)3s^1$  transition and peak 27 at a kinetic energy of 880.6 eV to the  $1s^{-2}3p^1 \rightarrow 1s^{-1}2p^{-2}(2D)3p^1$  transition. The assignment of peak 28 is in line with the calculations of Southworth *et al.* [36]; however, the similarly intense peak 27 is not reproduced by their calculations since they took only  $2S^e$  intermediate states into account.

One can extend this method to find the kinetic energy of hypersatellites corresponding to transitions involving a shake process. From Ref. [29] it is known that splitting between the states  $1s^{-2}4p^1$  and  $1s^{-2}3p^1$  amounts to  $\cong 5.7$  eV, which gives a kinetic energy of 886.636 eV. This suggests assigning peak 29 at 887.4 eV to the hypersatellite transition  $1s^{-2}4p^1 \rightarrow 1s^{-1}2p^{-2}(2D)3p^1$ , i.e., to a shake-down process.

### C. Hypersatellites of $K^{-2}L^{-1}$ and $K^{-2}L^{-1}V$ electronic states

In Fig. 3 the Auger decays of the  $K^{-2}L^{-1}$  are indicated in red filled with vertical lines and those of the  $K^{-2}L^{-1}V$  states in orange filled with diagonal lines going from top left to bottom right. In the fit analysis, these lines were described with a PCI line shape using an identical linewidth of  $\sim 750$  meV for all transitions; this linewidth resulted in a better agreement between the fit result and the spectrum than the linewidth of  $910 \pm 12$  meV used for the Auger decays of the  $K^{-2}$  state. The smaller linewidth as compared to the one used for the  $K^{-2}$  states is related to the vacancy in the  $L$  shell reducing the number of possible Auger decay channels. In more detail,

from the calculations of Bhalla *et al.* [43] we derived lifetime broadenings of 765 to 795 meV for the  $1s^{-2}2p^{-1}$  state and 805 to 835 meV for the  $1s^{-2}2s^{-1}$  state. These values are in reasonable agreement with  $\sim 750$  meV obtained in the fit analysis and the deviations are caused by different lifetimes for the  $1s^{-1}2(s,p)^{-3}$  final states. However, based on the statistics of the present spectra this linewidth argument could not be utilized in the fit analysis to distinguish the different Auger transitions.

The Auger decays of the  $K^{-2}L^{-1}$  and  $K^{-2}L^{-1}V$  states often imply three or more open shells, making it difficult to adapt the equivalent core-method described in the previous subsection in order to find the kinetic energies of the different transitions involved. However, this approach is still helpful to identify, for a given configuration, the different LS designations by using the corresponding energy difference between different LS designations of the respective equivalent-core atom.

To identify the different transitions we first performed *ab initio* calculations at the CASSCF level using the MOLPRO [47] quantum chemistry software. We used a Gaussian basis set, aug-cc-pCVTZ [48,49], to take into account core-core and core-valence correlation effects. We also included relativistic corrections using the Douglas-Kroll Hamiltonian [50,51]. As an important general result of our calculations we obtained that the  $K^{-2}L^{-1} \rightarrow K^{-1}L^{-3}$  are expected in the energy range of  $\sim 810$ – $845$  eV, while the  $K^{-2}L^{-1}V \rightarrow K^{-1}L^{-3}V$  are estimated to be found in the range of  $\sim 830$ – $865$  eV.

For a given configuration and a specified multiplicity  $2S+1$  the calculations provide different energy levels. To assign the transitions observed in Fig. 3 we identified the LS designations of these energy levels by employing the equivalent-core approximation. In this way the  $K^{-2}L^{-1}$  excited states of neon were assigned using the configurations  $1s^22s^22p^5$  and  $1s^22s^12p^6$  of  $Mg^{3+}$ . As shown in Fig. 1, the  $K^{-2}L^{-1}$  excited states can decay into the states  $K^{-1}L^{-3}$ , which can be compared with the configurations  $1s^22s^22p^3$ ,  $1s^22s^12p^4$ , and  $1s^22s^02p^5$  of  $Na^{4+}$ .

To identify the LS designations of the  $K^{-2}L^{-1}V$  excited states, we used the configurations  $1s^22s^12p^6V$  and  $1s^22s^22p^5V$  of  $Mg^{2+}$ . The resulting decay products  $K^{-1}L^{-3}V$  have at least three open shells that make using the equivalent core model impossible. However, the calculated energy differences of these states agree quite well with the energy differences of the  $L^{-3}V$  electronic states of  $Ne^{2+}$ . This shows that the  $1s$  electron has a very limited effect on the unpaired valence electrons. A similar observation has been made for the  $K^{-1}L^{-2}$  and the  $L^{-2}$  states of neon; see above. As a consequence, the LS designations of the calculated  $K^{-1}L^{-3}V$  states of  $Ne^{3+}$  can be identified with the  $L^{-3}V$  electronic states of  $Ne^{2+}$ .

In the following we shall first discuss the assignments of the  $K^{-2}L^{-1} \rightarrow K^{-1}L^{-3}$  Auger decays. Based on the selection rules for Auger decay (angular momentum and parity conservation) as well as by excluding spin flips, the electronic state  $1s^{-2}2s^{-1}(2S^e)$  can decay into the final states  $1s^{-1}2s^{-2}2p^{-1}(1,3P^o)$  and  $1s^{-1}2s^{-1}2p^{-2}(1,3S^e, 1,3D^e)$ . With the same arguments the state  $1s^{-2}2p^{-1}(2P^o)$  can decay into the final states  $1s^{-1}2s^{-2}2p^{-1}(1,3P^o)$ ,  $1s^{-1}2s^{-1}2p^{-2}(1,3S^e, 1,3P^e, 1,3D^e)$ , as

well as  $1s^{-1}2p^{-3}(^1,^3P^o, ^1,^3D^o)$ . We will first present the results obtained for the  $1s^{-2}2s^{-1}(^2S^e)$  state followed by those for the  $1s^{-2}2p^{-1}(^2P^o)$  state.

The calculations result in an Auger energy of 837.844 eV for the  $1s^{-2}2s^{-1}(^2S^e) \rightarrow 1s^{-1}2s^{-1}2p^{-2}(^1S^e)$  and of 844.073 eV for the  $1s^{-2}2s^{-1}(^2S^e) \rightarrow 1s^{-1}2s^{-1}2p^{-2}(^1D^e)$ . These values agree well with the experimental energies of peaks 8 and 14 summarized in Table I. The energy splitting of 6.229 eV between the two calculated transition energies agrees well with the energy difference of 6.550 eV between the states  $2s^12p^4(^2S)$  and  $2s^12p^4(^2D)$  of the  $Z + 1$  atom  $\text{Na}^{4+}$ , underlining the assignment [46].

Now we shall turn to the Auger decays of the  $1s^{-2}2p^{-1}(^2P^o)$  state. For the transitions  $1s^{-2}2p^{-1}(^2P^o) \rightarrow 1s^{-1}2s^{-1}2p^{-2}(^1S^e)$ ,  $1s^{-2}2p^{-1}(^2P^o) \rightarrow 1s^{-1}2s^{-1}2p^{-2}(^1D^e)$ , and  $1s^{-2}2p^{-1}(^2P^o) \rightarrow 1s^{-1}2p^{-3}(^1D^o)$  we obtained from the calculations kinetic energies of 810.905, 817.134, and 845.970 eV, respectively. These first two values agree well with the experimental kinetic energies of peaks 1 and 4. The kinetic energy of 845.970 eV for the transition  $1s^{-2}2p^{-1}(^2P^o) \rightarrow 1s^{-1}2p^{-3}(^1D^o)$  is quite close to the energy position of the transition  $1s^{-2} \rightarrow 1s^12s^12p^5\ ^3P^0(^2S)$ . The latter transition is significantly more intense than the calculated values and this misfit might be due to an unresolved overlap with the  $1s^{-2}2p^{-1}(^2P^o) \rightarrow 1s^{-1}2p^{-3}(^1D^o)$  transition. The energy splitting of 35.065 eV calculated for the final states  $1s^{-1}2p^{-3}(^1D)$  and  $1s^{-1}2s^{-1}2p^{-2}(^1S)$  agrees well with the splitting of 37.491 eV between the states  $2s2p^4(^2S)$  and  $2s^22p^3(^2D)$  of the  $Z + 1$  atom  $\text{Na}^{4+}$  [46].

In the following we will discuss the  $K^{-2}L^{-1}V \rightarrow K^{-1}L^{-3}V$  Auger transitions, which are in more detail:

$$\begin{aligned} 1s^{-2}2s^{-1}V &\rightarrow 1s^{-1}2s^{-2}2p^{-1}V \\ &\rightarrow 1s^{-1}2s^{-1}2p^{-2}V, \\ 1s^{-2}2p^{-1}V &\rightarrow 1s^{-1}2s^{-2}2p^{-1}V \\ &\rightarrow 1s^{-1}2s^{-1}2p^{-2}V \\ &\rightarrow 1s^{-1}2p^{-3}V. \end{aligned}$$

For the calculations we only took into account the states with  $V = 3s$  or  $3p$ , i.e., we considered only spectator Auger decays and neglected excitation into higher Rydberg orbitals as well as shake transitions.

As mentioned above, the term values of the  $K^{-2}L^{-1}V$  were derived by comparing with the equivalent core atom  $\text{Mg}^{2+}$ , revealing similar splittings. For example, the calculated splitting of 0.103 eV between the  $1s^{-2}2p^{-1}3p(^1D)$  and the  $1s^{-2}2p^{-1}3p(^1P)$  excited states agrees well with the splitting of 0.116 eV between the corresponding states of  $\text{Mg}^{2+}$  [46]. The same holds for the splitting of 0.893 eV between the states  $1s^{-2}2p^{-1}3p(^3S)$  and  $1s^{-2}2p^{-1}3p(^3D)$ , which matches well the splitting of 0.888 eV between the  $\text{Mg}^{2+}$  states  $2p^{-1}3p(^3S)$  and  $2p^{-1}3p(^3D)$ ; for the latter state we used the weighted average of the  $^3D_J$  levels with  $J = 3, 2, 1$  [46].

The kinetic energies of the hypersatellite Auger transitions  $1s^{-2}2p^{-1}3p(^3S) \rightarrow 1s^{-1}2p^{-3}p(^2S)$  and  $1s^{-2}2p^{-1}3p(^3S) \rightarrow 1s^{-1}2p^{-3}p(^2P)$  were calculated to be 857.771 eV and 864.185 eV, respectively; these values agree well with the kinetic energies of peaks 23 and 24. Moreover, the calculated energy difference of 6.414 eV

agrees reasonably well with the difference of 5.956 eV between the states  $2p^{-3}3p(^3S)$  and  $2p^{-3}3p(^3P)$  of  $\text{Ne}^{2+}$  confirming the assignment. In addition, the calculated kinetic energies of 851.769 and 852.310 eV for, respectively, the  $1s^{-2}2p^{-1}3p(^3D) \rightarrow 1s^{-1}2s^{-1}2p^{-2}3p(^4D)$  and the  $1s^{-2}2p^{-1}3s(^3P) \rightarrow 1s^{-1}2s^{-1}2p^{-2}3s(^4P)$  transitions could correspond to the peaks 18 and 21. However, as mentioned above, the only valence orbitals taken into account were the  $3s$  and  $3p$  ones, so that we cannot exclude that these two peaks correspond to other transitions involving higher Rydberg orbitals.

In the following we shall discuss the assignments of the peaks 2, 5, 6, 7, and 10. In this context we want to point out that the calculated energy values obtained for final states with two holes in the  $2s$  orbital are not accurate enough to obtain conclusive assignments. As a consequence, the assignments of the discussed peaks are only tentative and marked in Table I with “?”.

The calculated energy difference between the intermediate states  $1s^{-2}2s^{-1}3s(^1S)$  and  $1s^{-2}2p^{-1}3s(^1P)$  is 25.078 eV. A participator Auger decay of these two states can lead to the final states  $1s^{-1}2s^{-2}(^2S)$  and  $1s^{-1}2s^{-1}2p^{-1}(^2P)$ , which have a calculated splitting of 28.844 eV. By assuming for the two final states that the same energy is required for an additional  $2p \rightarrow 3s$  excitation we obtain  $E(1s^{-1}2s^{-2}(^2S)) - E(1s^{-1}2s^{-1}2p^{-1}(^2P)) \approx E(1s^{-1}2s^{-2}2p^{-1}(^1P)3s) - E(1s^{-1}2s^{-1}2p^{-2}(^1D)3s)$  and find for the decay  $1s^{-2}2s^{-1}3s(^1S) \rightarrow 1s^{-1}2s^{-2}2p^{-1}(^1P)3s$  a transition energy of 837.273 eV which matches reasonably well the kinetic energy of peak 10.

In the same way, namely by assuming that the energy difference between the final states  $1s^{-1}2s^{-2}2p^{-1}(^1P)$  and  $1s^{-1}2s^{-1}2p^{-2}(^1D)$  is identical to that of the final states  $1s^{-1}2s^{-2}(^2S)$  and  $1s^{-1}2s^{-1}2p^{-1}(^2P)$ , i.e., that the additional  $2p$  ionization energy is identical for the last two cases, we find that the electron kinetic energy for the transition  $1s^{-2}2s^{-1}(^2S) \rightarrow 1s^{-1}2s^{-2}2p^{-1}(^1P)$  is 815.229 eV close to the kinetic energy of peak 2. A different approach using the equivalent-core approximation supports this assignment. In this approach, the energy difference between the states  $2s2p^4(^2S)$  and  $2p^5(^2P)$  of  $\text{Na}^{4+}$  amounts to 27.181 eV [46] and results in a kinetic energy of 810.663 eV for the transition  $1s^{-2}2s^{-1}(^2S) \rightarrow 1s^{-1}2s^{-2}2p^{-1}(^1P)$ ; this value is also relatively close to the kinetic energy of peak 2. Finally, following the same idea, the peaks 5, 6, and 7 could correspond to  $1s^{-2}2s^{-1}3p \rightarrow 1s^{-1}2s^{-2}2p^{-1}3p$  transitions.

#### D. Hypersatellites of the $K^{-2}L^{-1}V^2$ double shake-up states

Due to the strong Auger decays of the  $K^{-2}L^{-1}$  and  $K^{-2}L^{-1}V$  states one may also expect the hypersatellites of the  $K^{-2}L^{-1}V^2$  double shake-up states. However, such transitions are not observed and we shortly want to shed light on this fact. A comparison of the peak intensity resulting from the Auger decay of  $K^{-2}$  states (blue peaks filled with horizontal lines in Fig. 3) and  $K^{-2}V$  states (black peaks) shows that shake off is much more likely than shake up. Based on the observations for argon where the  $1s^{-1}2p^{-1}3p^{-1}V^2$  double shake-up states are significantly less intense than the  $1s^{-1}2p^{-1}V$  single shake-up states [28], one can expect that this also holds for neon. From

this we can conclude that the Auger decays of the double shake-up states are significantly less intense than the black peaks caused by the decay of the  $K^{-2}V$  states. Finally, we want to point out that in the ionization process only one fast photoelectron is leaving the atom so that symmetric line shape is expected for these decays due to a very weak PCI effect; lines that fulfill their criteria are clearly assigned to  $K^{-2}V$  Auger decays.

### E. Satellites of $K^{-1}L^{-1}V$ electronic states

The green peaks filled with diagonal lines going from bottom left to top right in Fig. 3 are assigned to participator Auger decays of the shake-up satellites accompanying the Ne  $1s^{-1}$  ionization. Obviously, they overlap with the hypersatellites of the double-core-hole states. These types of  $1s^{-1}2p^{-1}np \rightarrow 2p^{-2}$  participator Auger decays have been observed before by Krause *et al.* [52] and can be readily identified in the fit analysis for two reasons. First, they show a Lorentzian line shape with a lifetime broadening much smaller than that of the DCH states but close to those of the single core-hole states of 242 meV [29,41]. Second, the Auger energies of the participator decays,  $E_{\text{Aug,part}}(np)$ , can be calculated based on simple energy arguments using the binding energies of the  $1s^{-1}2p^{-1}np$  shake-up satellites  $E_b(np)$ , the binding energy of the  $1s$  electron  $E_b(1s^{-1})$ , and the Auger energy of the  $1s^{-1} \rightarrow 2p^{-2}(^1D)$  transition  $E_{\text{Aug}}$ , namely

$$E_{\text{Aug,part}}(np) = E_{\text{Aug}} + E_b(np) - E_b(1s^{-1}). \quad (2)$$

In this context the values for  $E_b(np)$  are taken from Ref. [53] and the results show an excellent agreement with the fit results; see Table I. In detail, we found the  $1s^{-1}2p^{-1}np(L) \rightarrow 2p^{-2}(^1D_2)$  and  $1s^{-1}2p^{-1}np(H) \rightarrow 2p^{-2}(^1D_2)$  transitions with  $n \leq 6$ . Here  $L$  ( $H$ ) stands for lower (higher) excitation energies, i.e., the Rydberg series converges towards the  $1s^{-1}2p^{-1}(^3P)$  [ $1s^{-1}2p^{-1}(^1P)$ ] double ionization threshold. Note that all  $1s^{-1}2p^{-1}np$  states have  $^2P$  symmetry so that  $1s^{-1}2p^{-1}np(L)$  is predominately described by  $1s^{-1}2p^{-1}(^3P)np$ ; however, it is not identical to the latter state due to the admixing of some  $1s^{-1}2p^{-1}(^1P)np$ . The same holds for  $1s^{-1}2p^{-1}np(H)$  and  $1s^{-1}2p^{-1}(^1P)np$ . Note that the  $1s^{-1}2p^{-1}5p(L) \rightarrow 2p^{-2}(^1D_2)$  transition overlaps with peak 18, thus our fit analysis does not show any intensity for this decay. Moreover, the transition  $1s^{-1}2p^{-1}6p(H) \rightarrow 2p^{-2}(^1D_2)$  was too weak to be observed. In addition, we observed the  $1s^{-1}2p^{-1}3p(L, H) \rightarrow 2p^{-2}(^1S_0)$  participator Auger transitions. Interestingly, the  $1s^{-1}2p^{-1}3p(L) \rightarrow 2p^{-2}(^1S_0)$  to  $1s^{-1}2p^{-1}3p(L) \rightarrow 2p^{-2}(^1D_2)$  intensity ratio agrees within the error bars with the  $1s^{-1} \rightarrow 2p^{-2}(^1S_0)$  to  $1s^{-1} \rightarrow 2p^{-2}(^1D_2)$  intensity ratio of  $\cong 1 : 9$ .

### F. Branching ratios

Table III summarizes the relative intensities of the  $K^{-1}L^{-1}V$ ,  $K^{-2}$ ,  $K^{-2}V$ ,  $K^{-2}L^{-1}$ , and  $K^{-2}L^{-1}V$  Auger decays as obtained from the present fit analysis and assignment. The values are scaled so that the sum of all  $K^{-2}$  decay channels, i.e., the decay channels  $K^{-2}$ ,  $K^{-2}V$ ,  $K^{-2}L^{-1}$ , and  $K^{-2}L^{-1}V$ , is equal to 100. The energy region presented in Figs. 2 and 3 corresponds to the essential part of the energy

TABLE III. Relative intensities of the different decay channels as obtained from the fit analysis and the assignment. The intensities are scaled so that the sum of the decay channels  $K^{-2}$ ,  $K^{-2}V$ ,  $K^{-2}L^{-1}$ , and  $K^{-2}L^{-1}V$  is equal to 100.

Decay channel	Rel. intensities
$K^{-1}L^{-1}V$	25
$K^{-2}$	57
$K^{-2}V$	4
$K^{-2}L^{-1}$	16
$K^{-2}L^{-1}V$	23

regions where the different  $K^{-2}$  decay channels are expected. For this reason the given branching ratios can be considered as rough estimates of the production of  $K^{-2}$ ,  $K^{-2}V$ ,  $K^{-2}L^{-1}$ , and  $K^{-2}L^{-1}V$  states. At low kinetic energy ( $<810$  eV), the most probable DCH states should be  $K^{-2}L^{-1}$ , which means that this decay channel may be underestimated in the present study.

The numbers in Table III show that about 61% of the DCH states decays, namely from the  $K^{-2}$  and the  $K^{-2}V$  electronic states, are single shake processes. The remaining 39% are due to double-shake processes corresponding to the states  $K^{-2}L^{-1}$  and  $K^{-2}L^{-1}V$ . Obviously, in the case of a single-shake process the shake-off is dominant (over 90%). In about 40% of the double-shake processes both electrons are promoted to the continuum, while in about 60% of the processes only one electron is promoted to the continuum. In contrast, double-shake-up processes with two electrons promoted into a discrete level are not observed in the present study.

From our fit analysis we determined the intensity ratio of the  $1s^{-2} \rightarrow 1s^{-1}2p^{-2}(^2D)$  hypersatellite to the  $1s^{-1} \rightarrow 2p^{-2}(^1D)$  to be 0.00090(5). This value is significantly smaller than the value of 0.00223(10) given by Southworth *et al.* [36]. Following the argumentation of Southworth *et al.* but using the present branching ratio for the  $1s^{-2} \rightarrow 1s^{-1}2p^{-2}(^2D)$  of 0.543 corrected by 0.9 for the single Auger yield we obtain a ratio of 0.00111(20) for the double to single ionization yield, compared to 0.0032(4) of Southworth *et al.* [36].

In a complementary approach we determined the ratio of  $K^{-2}$  and  $K^{-1}$  core-hole creation, i.e., shake processes accompanying the  $K$ -hole creation are also taken into account. In this approach we determined in a first step the fraction of intensity of the  $K^{-1}L^{-1}V$  spectator decays on the entire  $KLL$  Auger spectrum and obtained a value of 0.00030(6). Here, the large error bar is due to the different systematic errors like background correction. Assuming again a single Auger yield for the  $K^{-2}$  states of 0.9 and an intensity ratio of 4.0(0.4) for the sum of all  $K^{-2}$  Auger decays to the  $K^{-1}L^{-1}V$  spectator decays, see Table III with the error bar reflecting the systematic errors due to unresolved overlapping lines, we obtain for the ratio of the  $K^{-2}$  and  $K^{-1}$  core-hole creation of 0.00133(50), in good agreement with the value given above.

Although the two values derived in this work describe slightly different quantities, they are similar to each other but much smaller than the value of 0.0032(4) provided in [36] for the double to single ionization yield. However, contrary to the

experiments of Southworth *et al.* [36], which were performed using a photon energy of 5 keV, the present experiments were performed with 2.3 keV photons. As a result, the photoelectrons have a maximal kinetic energy around 450 eV so that the experiment is not performed in the *sudden limit*. As a result, in the Thomas model a further increase of the shake probability with the photon energy is expected [54].

#### IV. SUMMARY AND CONCLUSIONS

In summary, we have presented the hypersatellite Auger spectrum of neon which contains the decay transitions of the  $K^{-2}$ , the  $K^{-2}V$ , the  $K^{-2}L^{-1}$ , the  $K^{-2}L^{-1}V$ , and the  $K^{-1}L^{-1}V$  states. High experimental resolution available in the present work allows for distinguishing the Auger decay of different types of core-hole states based on their linewidths and line shapes. A detailed assignment of the different transitions is based on various approaches including calculations and the equivalent-core approximation. In particular, we have performed complementary calculations to assign the  $K^{-2}L^{-1} \rightarrow K^{-1}L^{-3}$  and the  $K^{-2}L^{-1}V \rightarrow K^{-1}L^{-3}V$  Auger transitions. Based on the obtained results a ratio of 0.00111(20) for the double to single ionization yield is derived. This value is much smaller than the ratio of 0.0032(4) obtained by Southworth *et al.* [36]; however, it might be explained by different ionization energies.

In conclusion, we show the high complexity of the hypersatellite Auger spectrum of neon due to the different decay processes. These results might be helpful to understand the hypersatellite Auger spectra of molecules containing second-row elements like fluorine or oxygen; these spectra are expected to consist of the same types of decay processes. However, within a few femtoseconds these decay processes create multiply charged molecular ions with molecular charge states up to 4+ or 5+ which are expected to be highly dissociative. The additional degree of freedom of the nuclear dynamics will probably further complicate the physical picture. However, it may also open the opportunity to study ultrafast dissociation of highly charged molecular ions.

#### ACKNOWLEDGMENTS

Experiments were performed on the GALAXIES beamline at SOLEIL Synchrotron, France (Proposal No. 99140145). We are grateful to D. Prieur for technical assistance and to SOLEIL staff for smoothly running the facility. A.F.L. thanks Coordenação de Aperfeiçoamento de Pessoal de Nível Superior–Brazil for the support. I.I. acknowledges financial support from Labex Plas@Par. B.C.d.M. acknowledges financial support from ANR SUMMIT.

- 
- [1] R. Neutze, R. Wouts, D. van der Spoel, E. Weckert, and J. Hajdu, *Nature (London)* **406**, 752 (2000).
  - [2] O. Travnikova, T. Marchenko, G. Goldsztejn, K. Jänkälä, N. Sisourat, S. Carniato, R. Guillemin, L. Journal, D. Céolin, R. Püttner *et al.*, *Phys. Rev. Lett.* **116**, 213001 (2016).
  - [3] G. Charpak, C. R. Hebd. Seances Acad. Sci. **237**, 243 (1953).
  - [4] J. P. Briand, P. Chevallier, M. Tavernier, and J. P. Rozet, *Phys. Rev. Lett.* **27**, 777 (1971).
  - [5] P. Richard, W. Hodge, and C. F. Moore, *Phys. Rev. Lett.* **29**, 393 (1972).
  - [6] D. J. Nagel, A. R. Knudson, and P. G. Burkhalter, *J. Phys. B* **8**, 2779 (1975).
  - [7] L. M. Kiernan, E. T. Kennedy, J.-P. Mosnier, J. T. Costello, and B. F. Sonntag, *Phys. Rev. Lett.* **72**, 2359 (1994).
  - [8] J.-P. Briand, L. de Billy, P. Charles, S. Essabaa, P. Briand, R. Geller, J. P. Desclaux, S. Bliman, and C. Ristori, *Phys. Rev. Lett.* **65**, 159 (1990).
  - [9] J.-P. Briand, L. de Billy, P. Charles, S. Essabaa, P. Briand, R. Geller, J. P. Desclaux, S. Bliman, and C. Ristori, *Phys. Rev. A* **43**, 565 (1991).
  - [10] J. Limburg, J. Das, S. Schippers, R. Hoekstra, and R. Morgenstern, *Phys. Rev. Lett.* **73**, 786 (1994).
  - [11] J. Limburg, S. Schippers, I. Hugues, R. Hoekstra, R. Morgenstern, S. Hustedt, N. Hatke, and W. Heiland, *Nucl. Instrum. Methods, Phys. Res. B* **98**, 436 (1995).
  - [12] O. Keski-Rahkonen, J. Saijonmaa, M. Suvanén, and A. Servomaa, *Phys. Scr.* **16**, 105 (1977).
  - [13] R. Wehlitz, F. Heiser, O. Hemmers, B. Langer, A. Menzel, and U. Becker, *Phys. Rev. Lett.* **67**, 3764 (1991).
  - [14] L. Journal, D. Cubaynes, J.-M. Bizau, S. Al Moussalami, B. Rouvellou, F. J. Wuilleumier, L. VoKy, P. Faucher, and A. Hibbert, *Phys. Rev. Lett.* **76**, 30 (1996).
  - [15] L. Young, E. P. Kanter, B. Krässig, Y. Li, A. M. March, S. T. Pratt, R. Santra, S. H. Southworth, N. Rohringer, L. F. DiMauro *et al.*, *Nature (London)* **466**, 56 (2010).
  - [16] N. Berrah, L. Fang, B. Murphy, T. Osipov, K. Ueda, E. Kukk, R. Feifel, P. van der Meulen, P. Salen, H. T. Schmidt *et al.*, *Proc. Natl. Acad. Sci. USA* **108**, 16912 (2011).
  - [17] P. Salen, P. van der Meulen, H. T. Schmidt, R. D. Thomas, M. Larsson, R. Feifel, M. N. Piancastelli, L. Fang, B. Murphy, T. Osipov *et al.*, *Phys. Rev. Lett.* **108**, 153003 (2012).
  - [18] J. H. D. Eland, M. Tashiro, P. Linusson, M. Ehara, K. Ueda, and R. Feifel, *Phys. Rev. Lett.* **105**, 213005 (2010).
  - [19] P. Lablanquie, F. Penent, J. Palaudoux, L. Andric, P. Selles, S. Carniato, K. Bučar, M. Žitnik, M. Huttula, J. H. D. Eland *et al.*, *Phys. Rev. Lett.* **106**, 063003 (2011).
  - [20] P. Lablanquie, T. P. Grozdanov, M. Žitnik, S. Carniato, P. Selles, L. Andric, J. Palaudoux, F. Penent, H. Iwayama, E. Shigemasa *et al.*, *Phys. Rev. Lett.* **107**, 193004 (2011).
  - [21] M. Tashiro, M. Nakano, M. Ehara, F. Penent, L. Andric, J. Palaudoux, K. Ito, Y. Hikosaka, N. Kouchi, and P. Lablanquie, *J. Chem. Phys.* **137**, 224306 (2012).
  - [22] M. Nakano, P. Selles, P. Lablanquie, Y. Hikosaka, F. Penent, E. Shigemasa, K. Ito, and S. Carniato, *Phys. Rev. Lett.* **111**, 123001 (2013).
  - [23] M. Mucke, J. H. D. Eland, O. Takahashi, P. Linusson, D. Lebrun, K. Ueda, and R. Feifel, *Chem. Phys. Lett.* **558**, 82 (2013).
  - [24] S. Carniato, P. Selles, L. Andric, J. Palaudoux, F. Penent, M. Žitnik, K. Bučar, M. Nakano, Y. Hikosaka, K. Ito *et al.*, *J. Chem. Phys.* **142**, 014307 (2015).
  - [25] S. Carniato, P. Selles, L. Andric, J. Palaudoux, F. Penent, M. Žitnik, K. Bučar, M. Nakano, Y. Hikosaka, K. Ito *et al.*, *J. Chem. Phys.* **142**, 014308 (2015).

- [26] S. Carniato, P. Selles, P. Lablanquie, J. Palaudoux, L. Andric, M. Nakano, Y. Hikosaka, K. Ito, T. Marchenko, O. Travnikova *et al.*, *Phys. Rev. A* **94**, 013416 (2016).
- [27] M. Žitnik, R. Püttner, G. Goldsztejn, K. Bučar, M. Kavčič, A. Mihelič, T. Marchenko, R. Guillemin, L. Journal, O. Travnikova, D. Céolin, M. N. Piancastelli, and M. Simon, *Phys. Rev. A* **93**, 021401(R) (2016).
- [28] R. Püttner, G. Goldsztejn, D. Céolin, J.-P. Rueff, T. Moreno, R. K. Kushawaha, T. Marchenko, R. Guillemin, L. Journal, D. W. Lindle *et al.*, *Phys. Rev. Lett.* **114**, 093001 (2015).
- [29] G. Goldsztejn, T. Marchenko, R. Püttner, L. Journal, R. Guillemin, S. Carniato, P. Selles, O. Travnikova, D. Céolin, A. F. Lago *et al.*, *Phys. Rev. Lett.* **117**, 133001 (2016).
- [30] J. Ahopelto, E. Rantavuori, and O. Keski-Rahkonen, *Phys. Scr.* **20**, 71 (1979).
- [31] E. P. Kanter, R. W. Dunford, B. Krässig, and S. H. Southworth, *Phys. Rev. Lett.* **83**, 508 (1999).
- [32] R. Diamant, S. Huotari, K. Hämäläinen, C. C. Kao, and M. Deutsch, *Phys. Rev. A* **62**, 052519 (2000).
- [33] Ž. Šmit, M. Žitnik, L. Avaldi, R. Camilloni, E. Fainelli, A. Mühleisen, and G. Stefani, *Phys. Rev. A* **49**, 1480 (1994).
- [34] P. Pelicon, I. Čadež, M. Žitnik, Ž. Šmit, S. Dolenc, A. Mühleisen, and R. I. Hall, *Phys. Rev. A* **62**, 022704 (2000).
- [35] M. Oura, H. Yamaoka, K. Kawatsura, K. Takahiro, N. Takeshima, Y. Zou, R. Hutton, S. Ito, Y. Awaya, M. Terasawa, T. Sekioka, and T. Mukoyama, *J. Phys. B* **35**, 3847 (2002).
- [36] S. H. Southworth, E. P. Kanter, B. Krässig, L. Young, G. B. Armen, J. C. Levin, D. L. Ederer, and M. H. Chen, *Phys. Rev. A* **67**, 062712 (2003).
- [37] J.-P. Rueff, J. M. Ablett, D. Céolin, D. Prieur, T. Moreno, V. Balédent, B. Lassalle-Kaiser, J. E. Rault, M. Simon, and A. Shukla, *J. Synchrotron Radiat.* **22**, 175 (2015).
- [38] D. Céolin, J. M. Ablett, D. Prieur, T. Moreno, J.-P. Rueff, T. Marchenko, L. Journal, R. Guillemin, B. Pilette, T. Marin *et al.*, *J. Electron Spectrosc. Relat. Phenom.* **190**, 188 (2013).
- [39] J. A. R. Samson, *Rev. Sci. Instrum.* **40**, 1174 (1969).
- [40] M. Simon, R. Püttner, T. Marchenko, R. Guillemin, R. K. Kushawaha, L. Journal, G. Goldsztejn, M. N. Piancastelli, J. M. Ablett, J.-P. Rueff *et al.*, *Nat. Commun.* **5**, 4069 (2014).
- [41] V. G. Yarzhemsky and A. Sgamellotti, *J. Electron Spectrosc. Relat. Phenom.* **125**, 13 (2002).
- [42] H. Aksela, S. Aksela, and H. Patana, *Phys. Rev. A* **30**, 858 (1984).
- [43] C. P. Bhalla, N. O. Folland, and M. A. Hein, *Phys. Rev. A* **8**, 649 (1973).
- [44] Y. Liu, J. Zeng, and J. Yuan, *J. Phys. B* **46**, 145002 (2013).
- [45] M. H. Chen, *Phys. Rev. A* **44**, 239 (1991).
- [46] NIST atomic spectra database energy levels, [http://physics.nist.gov/PhysRefData/ASD/levels\\_form.html](http://physics.nist.gov/PhysRefData/ASD/levels_form.html)
- [47] H.-J. Werner, P. J. Knowles, G. Knizia, F. R. Manby, and M. Schütz, *WIREs Comput. Mol. Sci.* **2**, 242 (2012).
- [48] T. H. Dunning, *J. Chem. Phys.* **90**, 1007 (1989).
- [49] D. E. Woon and T. H. Dunning, *J. Chem. Phys.* **98**, 1358 (1993).
- [50] M. Reiher and A. Wolf, *J. Chem. Phys.* **121**, 2037 (2004); **121**, 10945 (2004).
- [51] A. Wolf, M. Reiher, and B. A. Hess, *J. Chem. Phys.* **117**, 9215 (2002).
- [52] M. O. Krause, T. A. Carlson, and W. E. Moddeman, *J. Phys. Colloq.* **32**, C4-139 (1971).
- [53] S. Svensson, B. Eriksson, N. Mårtensson, G. Wendin, and U. Gelius, *J. Electron Spectrosc. Relat. Phenom.* **47**, 327 (1988).
- [54] T. D. Thomas, *Phys. Rev. Lett.* **52**, 417 (1984).